# The charge exchange recombination spectroscopy diagnostic on the upgraded Lithium Tokamak eXperiment (LTX-$\beta$)[a)]

D. B. Elliott,[1, b)] T. M. Biewer,[1] D. P. Boyle,[2] R. Kaita,[2] and R. Majeski[2]
[1)] *Oak Ridge National Laboratory, United States, P.O. Box 2008, Oak Ridge, TN 37831-6169*
[2)] *Princeton Plasma Physics Laboratory, United States, P.O. Box 451, Princeton, NJ 08543*

(Dated: 24 August 2018)

The Lithium Tokamak eXperiment has undergone an upgrade to LTX-$\beta$, a major part of which is the addition of neutral beam injection (NBI). NBI has allowed for a new charge exchange recombination spectroscopy (CHERS) system to be installed in order to measure impurity concentrations, ion temperature, and toroidal velocity. Previously on LTX measuring these parameters relied on passive spectroscopy and inversion techniques and had large uncertainty. The CHERS system has 52 total views, split into four groups of 13, half facing towards the beam and half symmetrically facing away from the beam so the background non-beam related emission can be simultaneously subtracted. Both sets of views sample a major radius of 27-59 cm, with resolution through the beam of 1.5-2.5 cm. LTX-$\beta$ is expected to have its magnetic axis near 35 cm, with minor radii of 18-23 cm. Three separate spectrometers will be used for the diagnostic, giving the system great flexibility to simultaneously measure emission from multiple impurity lines. The viewing optics are f/1.8, allowing all of the spectrometers to be fully illuminated. Design and calibration of the system as well as the advantages of various configurations of the spectrometers will be highlighted.

Keywords: Spectroscopy, Neutral Beam Injection, Charge Exchange, Optics

## I. INTRODUCTION

Many tokamaks have observed benefits from lithium wall conditioning[1–5] such as increased confinement time[6,7]. This has been attributed to lithium binding hydrogen, which reduces edge recycling. Recently, flat electron temperature profiles have been observed in the Lithium Tokamak eXperiment (LTX)[8]. This type of equilibrium has been described theoretically[9] and was suggested to come about from lithium coated walls and low neutral density in the scrape off layer[10]. The low recycling, hot edge, flat temperature profile regime is expected to have several advantages, such as greater confinement and reduction of thermal gradient driven modes.

Investigating and characterizing this new flat temperature regime will be the primary scientific goal of the upgraded LTX-$\beta$. A major part of the recent upgrade has been the integration of neutral beam injection (NBI) onto the experiment. NBI will allow for plasma heating, core fueling[11], apply an external torque[12], and enable the charge exchange recombination spectroscopy (CHERS)[13] diagnostic. Because edge fueling cools the plasma edge in the same way as recycling, core NBI fueling is required for the flat temperature regime to be extended in time. Flat temperature profiles are predicted for ions as well as electrons during a steady state low recycling regime, but were only observed for electrons in LTX. Applying a high external torque and observing the resultant toroidal velocity will test the prediction of low neutral drag due to low edge density.

Previous passive, impurity emission spectroscopy was available on LTX[14], but had limitations including being line integrated and unable to measure $Li^{3+}$. The CHERS measurements will be well localized and able to measure the temperature and velocity of $Li^{3+}$, therefore testing the previously mentioned predictions of plasma rotation and ion temperature profile. Because LTX-$\beta$ has steel plasma facing components which are coated in lithium, the major impurity species is expected to be lithium. This paper primarily considers CHERS based on fully ionized lithium, but the new system is also sensitive to emission from other impurities such as carbon and oxygen both previously observed in LTX.

In Sec. II, the LTX-$\beta$ upgrades and device parameters relevant to the CHERS diagnostic are discussed. The design of the CHERS mounting and optical systems are discussed in Sec. III along with the unique requirements of LTX-$\beta$. In Sec. IV the calibration of the CHERS system is described. The final section discusses the capabilities of the diagnostic, possible upgrades, and further measurements which can be made to improve the accuracy of the CHERS diagnostic.

## II. MACHINE DESCRIPTION

LTX-$\beta$ is expected to have plasmas of roughly equivalent spatial extent to those of LTX. The experiments of most interest, the flat temperature profile experiments, had typical major radii of 35-40 cm and a last closed flux surface near 60 cm[8]. The plasma current for many LTX discharges was $\sim$ 70 kA with durations of 20-30 ms and

[a)] Published as part of the Proceedings of the 22nd Topical Conference on High-Temperature Plasma Diagnostics, San Diego, California, April, 2018.

[b)] Author to whom correspondence should be addressed: delliott@pppl.gov

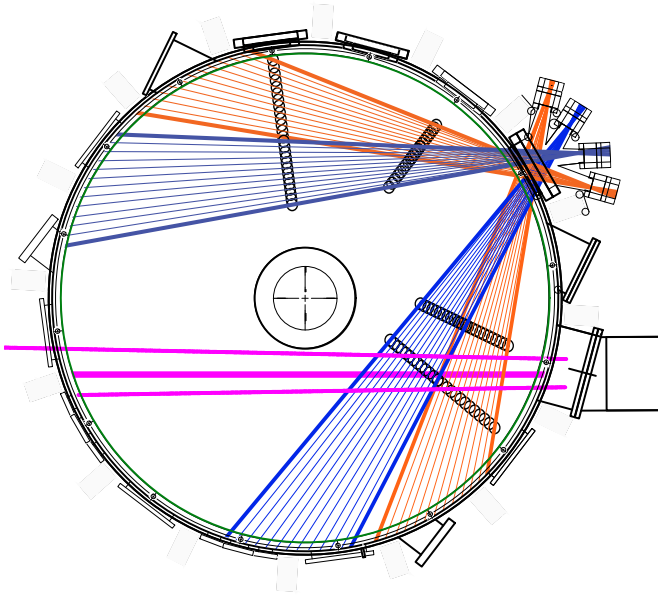

**FIG. 1:** A top down view of the LTX-$\beta$ device showing all 52 views. The solid blue and orange lines show each individual view, with colors corresponding to the core and edge respectively. The black circles are where the views were measured for spatial calibration. The magenta solid lines mark the location of the neutral beam.

peak electron temperatures of 200-300 eV[8]. In LTX-$\beta$, increased toroidal field as well as increased stored energy for ohmic heating will allow for extended pulse duration. The toroidal field will be approximately double of LTX, going from 0.17 T to 0.34 T. All of this should allow for 50-75 ms shots with toroidal current near 150 kA.

The upgrade most relevant to this work is the integration of a neutral beam system on loan from Tri-Alpha Energy, made by the Budker Institute of Nuclear Physics. The beam operates at 20 kV with a current of 35 A. Initial operation of neutral beam injection (NBI) will last for 5 ms. The power supplies, to operate for up to 16 ms are installed. The full energy fraction is specified at over 80%, but will be measured directly during operation. The beam divergence is $\leq 0.02$ rad. The tangency radius of the beam through LTX-$\beta$ is 21 cm which represents a limit on the innermost resolvable radii with the CHERS system. The NBI will add 700 kW of heating power, much more than the previous ohmic heating power of $\sim$150 kW. NBI will apply a significant external torque, which in the zero drag limit is calculated to lead to rotational frequencies of tens of kHz. Lastly, the NBI will add core fueling in plasmas with flat temperature profiles, thus extending the duration for which that regime can be maintained.

## III. COLLECTION OPTICS DESIGN

Designing a charge exchange spectroscopy system to cover a full minor radius of LTX-$\beta$ has several unique challenges including the lithium evaporation environment, the characteristics of the neutral beam, and the evolution of the plasma equilibrium. This section will define some of these challenges and the design choices made to overcome them or mitigate their impact.

The lithium evaporation environment poses a significant threat to viewports exposed to the plasma in LTX-$\beta$. The viewports need to be protected from evaporated lithium coatings, and must be replaceable without venting the machine. For this reason, each viewport is required to have a gate valve and a pump-out port in front of it. Ideally, the collection optics would have the largest possible aperture and be placed as close as possible to the plasma, so that their solid angle of collection and plasma coverage would both be maximized. However the width of gate valves increase with greater diameter, negating much of the benefits of larger optics. For this reason the thinnest possible valves (35 mm thick VAT 2.75 inch 010 series gate valves), custom viewports (with thinned steel and integrated pump out ports to shorten the optical assembly), and optics whose maximum aperture matches the aperture of the gate valve were chosen. All of these components can be seen in Fig. 2. These choices maximized the portion of the plasma which each set of views can sample, and protect the viewports from the harsh lithium environment.

In order to subtract the spontaneous emission of the plasma from the NBI induced charge exchange emission, each view facing the beam has a symmetric background view that points away from the beam and samples the same tangency radius of the plasma. Viewing the same tangency radii of the plasma from two different directions also allows for absolute wavelength calibration based on plasma emission, because Doppler shifts are equal and opposite for the counter facing views. This doubles the number of optical components and halves the available space for alignment systems, but allows simultaneous subtraction of spontaneous emission.

Previous LTX shots did not have active feedback control, and thus the plasma position and shape would evolve throughout the discharge. This necessitates a wide viewing range, machine radius of 30-60 cm, which can not be sampled with a single set of optics. In order to sample the entire region of interest two sets of views were used in each direction, two pointing towards the NBI and two pointing away.

In each direction, one set of views samples the core of the plasma, 27-43 cm, and the second set covers the edge, 43-59 cm, with some loss of throughput for the highest radii in each set of views. These views were chosen to cover the desired range and minimize the gap between sets of views. Each set has thirteen 660 $\mu m$, f/1.8 fibers, held in a fanned position with each fiber and view separated by 1 degree, whose throughput passes through a single lens. The core views, optimized for resolution and to minimize the gap between core and edge sets, have their light redirected by a mirror before being collected by the fibers. The mirrors allow the optical fibers to be redirected up and away from other diagnostics, and are susceptible to dust accumulation but were necessary to increase the viewing range without interfering with other systems. The edge views were chosen to access the greatest radii without leaving a gap between the core

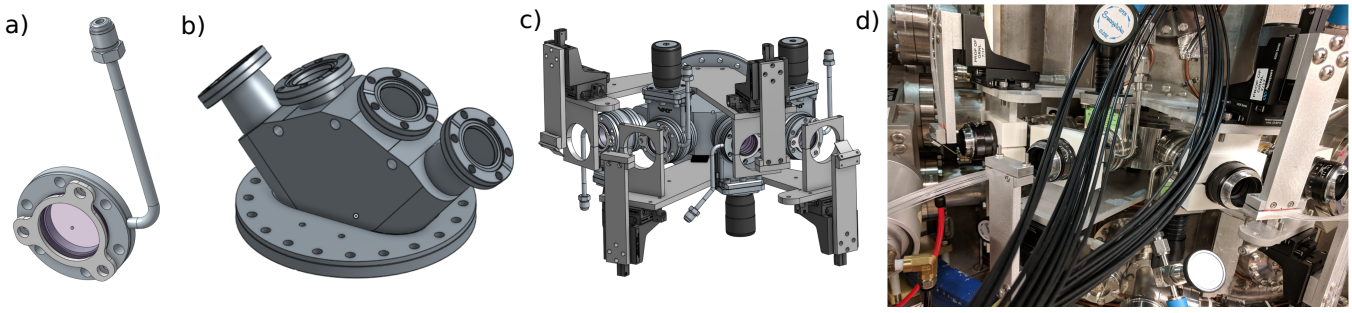


**FIG. 2:** Several opto-mechanical aspects of the LTX-$\beta$ CHERS system. From (a)-(d) the images are (a) a rendering of the thinned ported viewport; (b) the multi-directional port; (c) the complete opto-mechanical system sans the lenses; and (d) the fully installed system.

and edge sets of views. Three spectrometers are available for the CHERS system, an f/4.6 adjustable wavelength commercial Isoplane, an f/1.8 fixed grating commercial Holospec, and the f/1.8 High-throughput adjustable-wavelength lens-based (HAL) spectrometer[15,16]. In order to to fully illuminate the spectrometers, have minimal chromatic aberrations, keep the lens aperture close to the diameter of the viewport, and minimize the focal spot size of each view, f/1.8, 75 mm commercial camera lenses were selected for light collection.

As no single spectrometer can measure all of the 52 CHERS views, three spectrometers are being used each with its own advantages. The Holospec spectrometer has f/1.8 optics and a fixed grating and slit, so it has high throughput, reduced instrument width due to a curved slit, and calibration is simple and stable. The HAL spectrometer has f/1.8 optics and a tunable grating. This means the HAL spectrometer has both high throughput and can operate over a wide spectral range, but has fixed resolution for a given wavelength and spectral range. The Isoplane spectrometer has f/4.6 optics, three tunable gratings, and an adjustable slit. The optics give the Isoplane less throughput than the other two spectrometer. The selection of gratings, allow for the spectral range and resolution to be adjusted. All of these gratings are rotatable and thus the spectrometer can operate from 400 to 800 nm. The variable slit width also allows for resolution to be adjusted.

There are 52 views which sample 26 different radial locations, as can be seen in Fig. 3 part (a). The maximum number of views which can be sampled simultaneously by the spectrometers is 44. Between the two commercial spectrometers there are 21 inputs, and while HAL has a variable number of inputs its most numerous configuration has 23 inputs. Because the number of views is greater than can be sampled by the spectrometers, there is a fiber patch panel to select which views go into which spectrometer.

Having the fibers pass through a patch panel before entering the spectrometer has several operational advantages over terminating the collection fibers directly into the spectrometers. Because each spectrometer has advantages, the sampling can be optimized for different plasma scenarios. The fibers in these patch panels have their f-numbers match the spectrometers into which they are being terminated. For the f/4.6 spectrometer this means that the amount of stray light within the spectrometer is reduced without the amount of light reaching the photosensor being reduced. This lowers the noise within the system.

## IV. CALIBRATION

Three forms of calibration were performed on the LTX-$\beta$ optical system: spatial, throughput, and chromatic. The spatial calibration was performed only once and is the same regardless of spectrometer. The throughput and chromatic calibrations were performed for each spectrometer, so that the input fibers, internal through put, and differences in chromatic response could be taken into account.

In order to align and measure the position of the viewing chords, a ruled beam with 1 mm resolution was inserted through four different midplane ports, and positioned with 3D-printed jigs. Each fiber was back-illuminated and where the bright spots fell on the beam was recorded. Each view had two points defined this way, which defined each view. After both the beam facing and background views were initially measured, the background views were adjusted slightly to more symmetrically match the beam facing views. The location of each measurement point, and the determined viewing chords are shown in Fig. 1. It was also verified that each of these measured viewing paths passed through the optics, which acted as a third point to verify the measurements. The symmetric views have tangency radii which match each other to within 0.25 cm.

The tangency radii and beam intersection radii were calculated for each viewing chord and are shown in Fig. 3 (a). The beam intersection radii are near to the tangency radii, but are larger. The resolution of the CHERS system was also determined with these measurements. This is determined by the difference between the nearest and farthest machine radii which the view crosses while intersecting the beam. The resolution is given in Fig. 3 (b). In this figure, it is notable that the measured and predicted values for the CHERS resolution vary slightly. This is due to the virtual point, where the views intersect, being further in and slightly off center from the viewport. In the predictions, the virtual point was assumed to be in the center of the viewport. The core and edge views

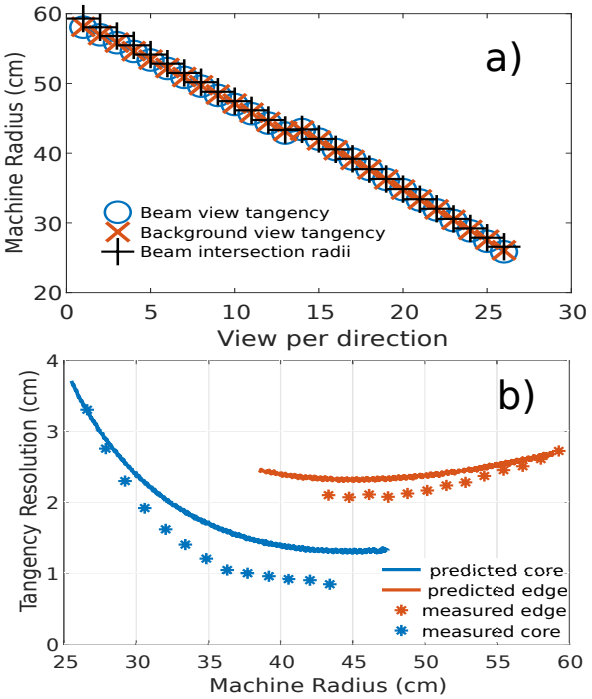


**FIG. 3:** The spatial calibration measurements are shown above. In part a) the close alignment between the tangency radii of the beam facing and background facing views (blue circles and orange X's respectively), as well as the beam crossing radii (black +'s) are shown. Part b) shows the resolution of each view through the beam, with measured values as *'s and predicted values as solid lines.

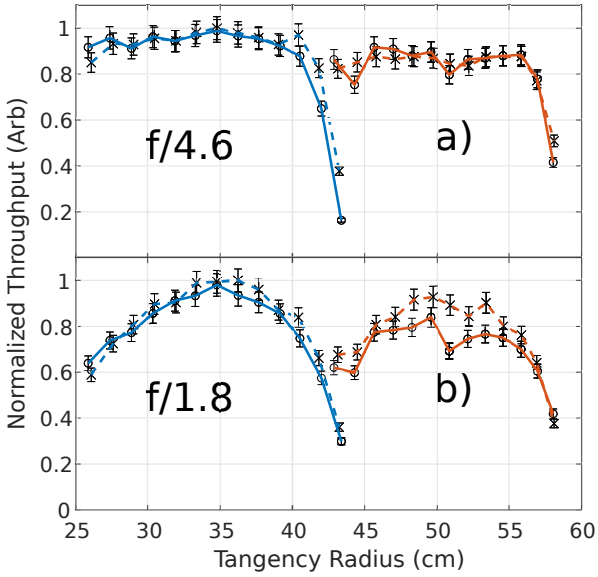


**FIG. 4:** The relative throughput for each view. Part a) was measured using the f/4.6 Isoplane , while part b) was measured using the f/1.8 Holospec. Dashed lines are the background facing views and solid lines denote the beam facing views. The blue curves are from the core facing view set and the orange the edge views. The error bars are based on the uncertainty in the uniformity of the integrating sphere and light source combination.

Table 1

| **Spectrometer** | **Resolution** | **Precision** | **f-number** |
|---|---|---|---|
| HAL | 0.09 nm | 0.0005 nm | 1.8 |
| Holospec | 0.09 nm | 0.01 nm | 1.8 |
| Isoplane | 0.08 nm | 0.01 nm | 4.6 |

allow for access to beam intersection radii of 26-59 cm, with resolution below 3 cm for the edge views and below 2 cm for 30-45 cm of the core views.

After the spatial calibration was determined, relative throughput calibration was performed for each of the views through each spectrometer. This was achieved by placing a small integrating sphere into the vessel with a flexible positioning arm, back illuminating each view and visually ensuring that the back illuminated spot was completely within the integrating sphere, then using a light emitting diode (LED) to illuminate the integrating sphere. This method ensured that each view was uniformly and equally illuminated. The relative throughput calibrations for the f/1.8 Holospec and the f/4.6 Isoplane are shown in Fig. 4.

There are two main trends to notice in the relative throughput data. The f/1.8 data has a view near the center of each lens through which the throughput is maximized, and the relative throughput is reduced near the edges of the lenses. The f/4.6 data is much flatter through a majority of the views. This is a result of the effective f-number changing for different views. The throughput difference would mean that the effective f-number for the view with the smallest tangency radius is f/2.2, if the decrease in relative throughput is completely due to effective f-number change. That slight change in f-number is supported by the f/4.6 data, which only sees variation in throughput at the far edges of the views where vignetting is expected.

Also, the viewing sets with higher tangency radius have lower throughput than their core counterparts. That decrease in throughput is due to the mirrors, which are used to redirect the path into the collection fibers. The mirrors reduce throughput by $\sim 10\%$. This drop in throughput can be seen in the difference between the maximum heights of the orange and blue curves in Fig. 4.

Along with the relative throughput calibrations, absolute sensitivity as a function of wavelength was determined for the 3 gratings in the Isoplane and the HAL spectrometer. For each calibration, spectra were collected from 400 to 800 nm while the light source and optics were varied in three configurations (1) through the entire CHERS system with the positionable integrating sphere and LED, (2) through only the patch panel fibers into the spectrometer with the LED integrating sphere, and (3) through the patch panel and spectrometer with a calibrated light source. From these measurements and the known output of the calibrated light source, the sensitivity of the CHERS system independent of light source was determined. It was found that the spectral response of the system varied less than the LED intensity uncertainty (%10) from 400 nm to 800 nm, for the CHERS optics and both spectrometers.

## V. ION TEMPERATURE AND VELOCITY MEASUREMENT CAPABILITIES

The Holospec has a fixed wavelength range, 511-521 nm, and so is optimized for sensitivity to the Li III $n = 7 - 5$ transition which emits at 516.69 nm. That is the transition many CHERS studies have looked at in the past[17,18]. The NBI on LTX-$\beta$ has a lower acceleration voltage than that in many other tokamaks, 20 keV, and thus the emission from the Li III $n = 5 - 4$ transition is 11 times as intense as the $n = 7 - 5$ transition of the NBI in LTX-$\beta$[19]. Both the Isoplane and HAL spectrometers can operate from 400 nm to above 800 nm, so they are sensitive to both transitions.

The sensitivity of the CHERS systems including sensor response and optical transmission was measured. The resulting relative sensitivity of the Isoplane, collection optics, and collection fibers to 516.69 nm radiation is nearly equivalent to that of 449.89 nm radiation. Therefore, the Isoplane is roughly 10 times more sensitive to the Li III $n = 5 - 4$ transition than the more traditional Li III $n = 7 - 5$ transition.

Since these measurements rely on the Doppler effect and the spectral resolution is nearly constant through wavelength, the velocity resolution is inversely proportional to the central wavelength of line emission and the temperature resolution is inversely related to the central wavelength squared. The temperature and plasma rotation resolution are therefore worse for the Li III $n = 5-4$ transition than for the Li III $n = 7-5$ transition, because of their wavelength difference. The temperature uncertainty is increased by 31% and the uncertainty in velocity is increased by 15% for the higher intensity, lower wavelength emission. Both transitions have their advantages, the $n = 7 - 5$ transition has higher precision in temperature and velocity, while the CHERS system is more sensitive to the $n = 5 - 4$ transition.

## VI. DISCUSSION

A new spectroscopy system has been installed on the recently upgraded LTX-$\beta$ to be used as a CHERS diagnostic. The design considerations and methods to prevent lithium coating damage were discussed. Spatial calibration, relative throughput calibrations, and absolute wavelength calibrations have all been performed on the system. The measured spatial calibration covers the designed region. The measured resolution is slightly better than the design due to optimized focusing and minimizing the view path lengths. The spatial calibrations show very good alignment with the beam facing and background views. The relative throughput calibration shows that the views not centered in the collection lens have a reduced effective f-number and that the mirrors used also reduced throughput. The wavelength calibration shows that while the system will be more sensitive to the shorter wavelength transition, the shorter wavelength will necessarily reduce the precision of the temperature and velocity measurements. This gives a choice of high sensitivity operation or high precision operation.

The optical systems have been installed and calibrated but there are still steps which can be taken to improve the CHERS system. Measurements of the NBI full, half, and third energy fractions will be performed. This can be done by firing the neutral beam into hydrogen gas and measuring the Doppler shifts of the emitted light. There is also an in-vessel beam dump calorimeter which will measure the fraction of the beam which shines through the plasma. This calorimeter will be calibrated so the calculations for the beam plasma interaction can be verified. Modeling is underway to predict the thermal response of the dump to NBI, and the dump can be experimentally calibrated by firing the NBI into an empty vacuum chamber and measuring the calorimeter response to the full beam energy.

## ACKNOWLEDGMENTS

This work is supported by US DOE contracts DE-AC02-09CH11466 and DE-AC05-00OR22725.

[1] H. W. Kugel *et al.*, Physics of Plasmas **15**, 056118 (2008).
[2] R. Maingi *et al.*, Fusion Engineering and Design **117**, 150 (2017).
[3] H. Guo *et al.*, Journal of Nuclear Materials **415**, S369 (2011), proceedings of the 19th International Conference on Plasma-Surface Interactions in Controlled Fusion.
[4] R. Maingi and EAST team, Nuclear Fusion **58**, 024003 (2018).
[5] H. Kugel *et al.*, Fusion Engineering and Design **85**, 865 (2010), proceedings of the 1st International Workshop on Lithium Applications for the Boundary Control in Fusion Devices.
[6] R. Maingi *et al.*, Phys. Rev. Lett. **107**, 145004 (2011).
[7] R. Majeski *et al.*, Phys. Rev. Lett. **97**, 075002 (2006).
[8] D. P. Boyle, R. Majeski, J. C. Schmitt, C. Hansen, R. Kaita, S. Kubota, M. Lucia, and T. D. Rognlien, Phys. Rev. Lett. **119**, 015001 (2017).
[9] P. J. Catto and R. D. Hazeltine, Physics of Plasmas **13**, 122508 (2006).
[10] S. Krasheninnikov, L. Zakharov, and G. Pereverzev, Physics of Plasmas **10**, 1678 (2003), https://doi.org/10.1063/1.1558293.
[11] H. K. Park *et al.*, Physics of Plasmas **4**, 1699 (1997).
[12] K.-D. Zastrow, W. Core, L.-G. Eriksson, M. V. Hellermann, A. Howman, and R. Knig, Nuclear Fusion **38**, 257 (1998).
[13] R. J. Fonck, R. J. Goldston, R. Kaita, and D. E. Post, Applied Physics Letters **42**, 239 (1983).
[14] T. K. Gray *et al.*, Review of Scientific Instruments **83**, 10D537 (2012).
[15] R. E. Bell and F. Scotti, Review of Scientific Instruments **81**, 10D731 (2010).
[16] F. Scotti and R. E. Bell, Review of Scientific Instruments **81**, 10D732 (2010).
[17] M. Podestà, R. Bell, A. Diallo, B. LeBlanc, F. Scotti, and the NSTX Team, Nuclear Fusion **52**, 033008 (2012).
[18] F. Scotti *et al.*, Nuclear Fusion **53**, 083001 (2013).
[19] H. P. Summers, The ADAS User Manual, version 2.6, http://www.adas.ac.uk (2004).

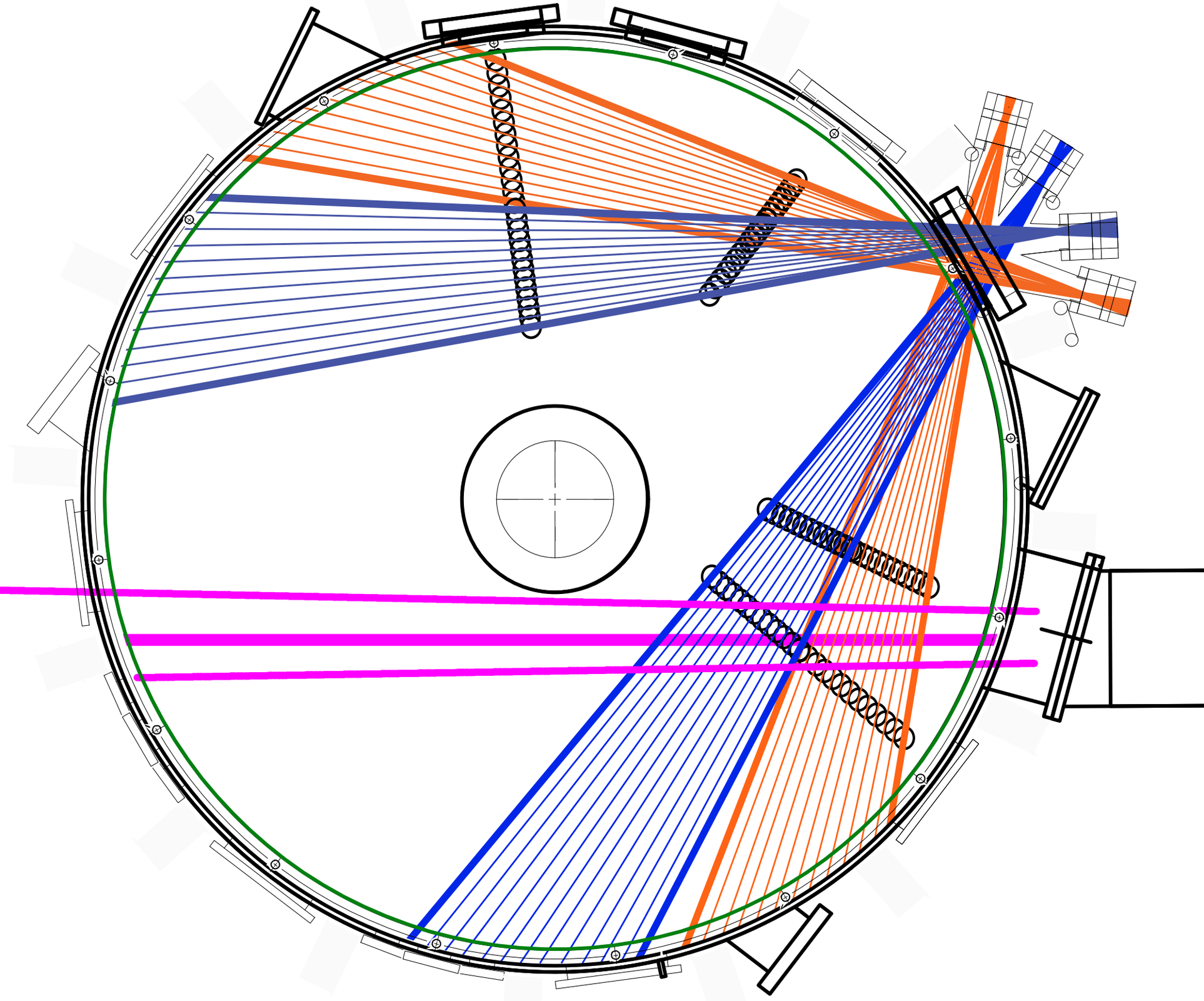

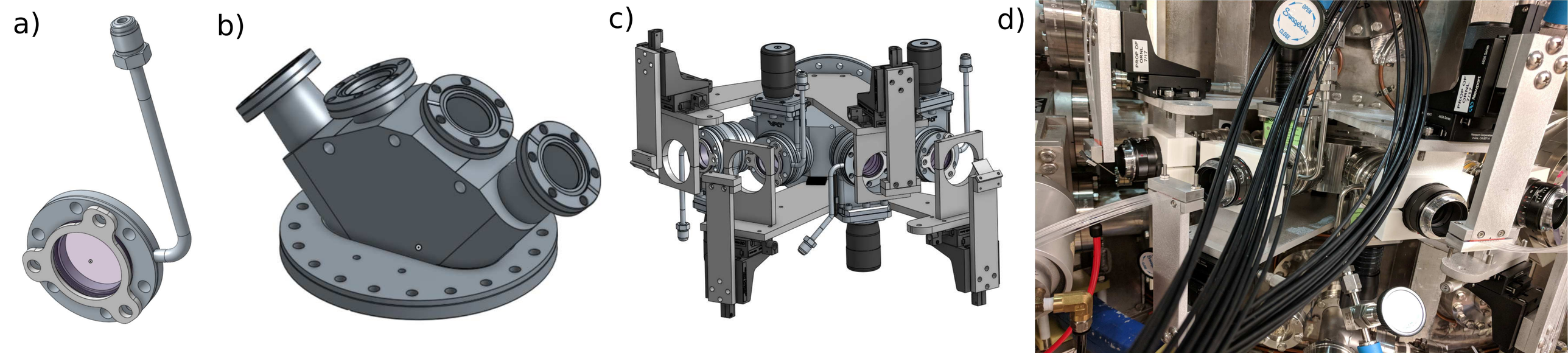
a)
b)
c)
d)

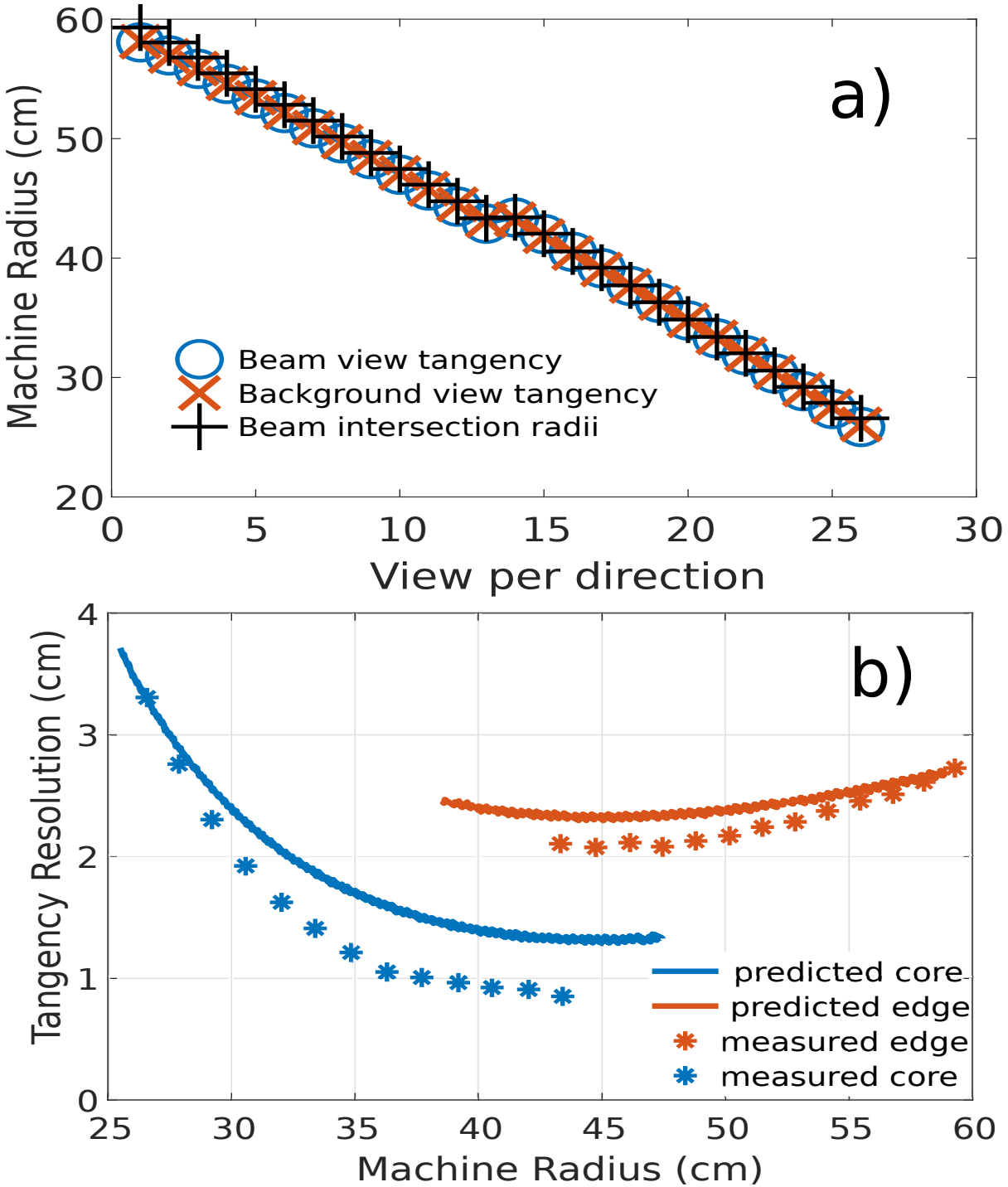
a)
Machine Radius (cm)
60
50
40
30
20
0
5
10
15
20
25
30
View per direction
Beam view tangency
Background view tangency
Beam intersection radii
b)
Tangency Resolution (cm)
4
3
2
1
0
25
30
35
40
45
50
55
60
Machine Radius (cm)
predicted core
predicted edge
measured edge
measured core

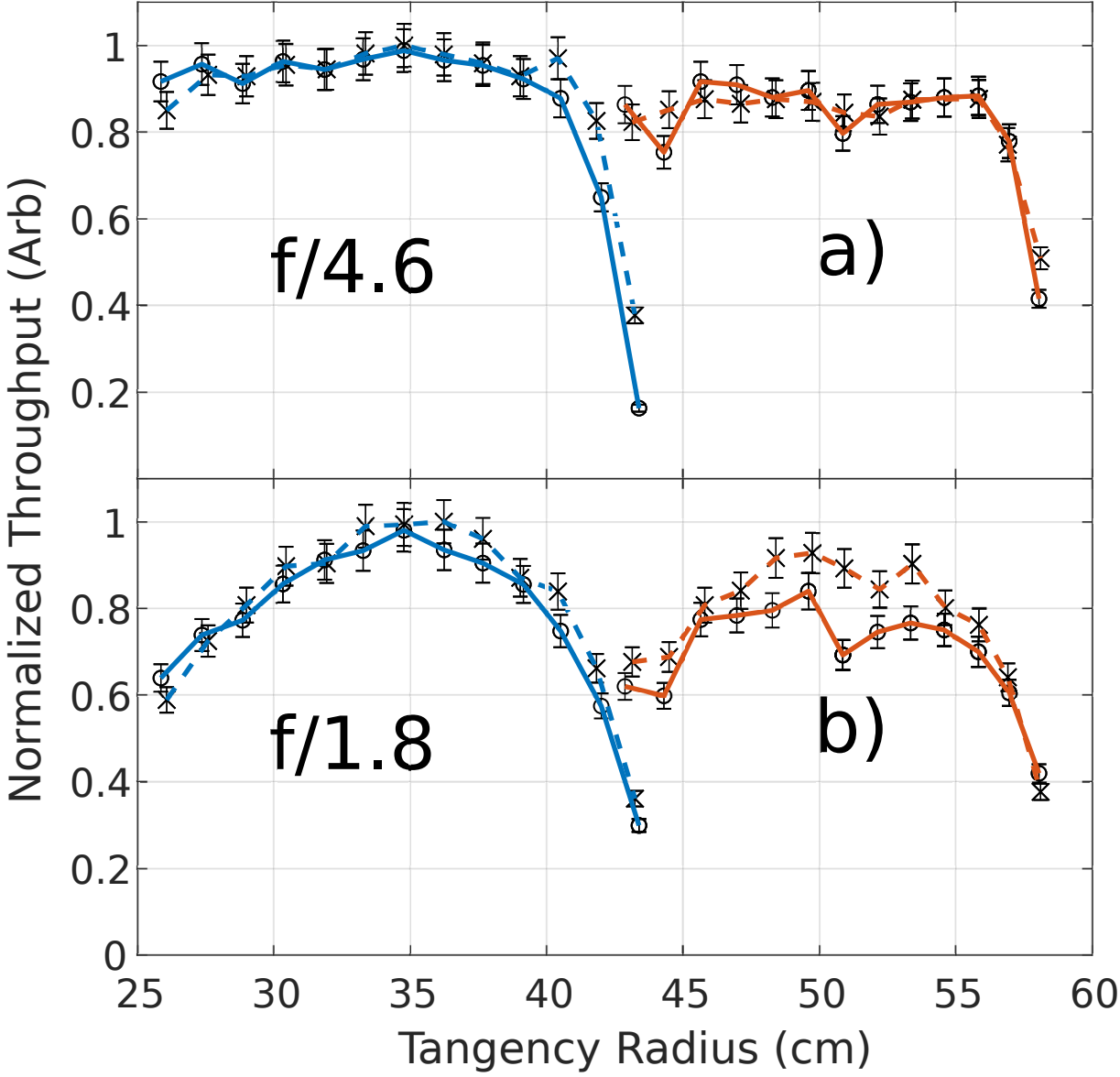
f/4.6
a)
f/1.8
b)
Normalized Throughput (Arb)
Tangency Radius (cm)
0
0.2
0.4
0.6
0.8
1
25
30
35
40
45
50
55
60